A Postprint of the WCNS-AO Scheme Based on Adaptive-Order Interpolation

Authors: Hu Yinggang

Date: 2025-11-01T21:55:05+00:00

Abstract

Euler equations constitute a class of typical nonlinear hyperbolic conservation laws, whose solutions may exhibit discontinuities. This characteristic causes high-order accurate numerical schemes for solving Euler equations to readily generate non-physical oscillations near discontinuities. A novel weighted compact nonlinear scheme (WCNS-AO) is developed for solving Euler equations based on the adaptive-order interpolation concept. Built upon the classical five-point WCNS scheme, this new scheme employs an adaptive-order nonlinear weighted interpolation technique that combines low-order interpolation on sub-stencils with high-order interpolation on the global stencil to enhance the performance of the original scheme. In the WCNS-AO scheme, spatial derivatives of flux at cell nodes are computed using a node-and-half-node hybrid sixth-order central difference scheme, while fluxes at cell interfaces are calculated via an adaptive-order nonlinear interpolation method in characteristic form. A high-order TVD Runge-Kutta method is utilized to solve the semi-discrete equations resulting from spatial discretization of the Euler equations. Numerical results demonstrate that the WCNS-AO scheme achieves the designed fifth-order accuracy in smooth regions, while exhibiting superior resolution and shock-capturing capabilities compared to the classical fifth-order WCNS-Z scheme and the fifth-order WENO-AO scheme.

Full Text

Preamble

Vol. 42 No. 5
Oct. 2025

Chinese Journal of Applied Mechanics DOI: 10.11776/j.issn.1000-4939.2025.05.018

A WCNS-AO Scheme Based on an Interpolation Method of Adaptive Order

HU Yinggang, JIANG Yanqun, HUANG Xiaoqian
(School of Mathematics and Physics, Southwest University of Science and Technology, 621010 Mianyang, China)

Abstract: The Euler equations represent a class of typical nonlinear hyperbolic conservation law equations whose solutions may contain discontinuities. This characteristic often leads to non-physical oscillations near discontinuities when high-order numerical schemes are employed to solve the Euler equations. This paper develops a novel weighted compact nonlinear scheme (WCNS-AO) for solving Euler equations based on the adaptive-order interpolation concept. Building upon the classical five-point WCNS scheme, this new scheme employs a nonlinear weighted interpolation technique that blends low-order interpolations on substencils with high-order interpolation on the global stencil to enhance performance. In the WCNS-AO scheme, spatial derivatives of fluxes at cell nodes are computed using a hybrid cell-edge and cell-node sixth-order central differencing scheme, while fluxes at cell interfaces are calculated via a characteristic-based nonlinear interpolation method with adaptive order. A high-order TVD Runge-Kutta method is used to solve the semi-discrete equations resulting from spatial discretization of the Euler equations. Numerical results demonstrate that the WCNS-AO scheme achieves fifth-order design accuracy in smooth regions and exhibits superior resolution and shock-capturing capability compared to the classical fifth-order WCNS-Z and WENO-AO schemes.

Keywords: Euler equations; adaptive order; WCNS-AO scheme; nonlinear interpolation; shock-capturing capability

CLC number: O354; O241
Document code: A
Article ID: 1000-4939(2025)05-1155-10

Introduction

The Euler equations play a crucial role in fluid mechanics. Their two-dimensional form is expressed as

$$U_t + F(U)_x + G(U)_y = 0$$

where $U = [\rho, \rho u, \rho v, E]^T$ represents the conservative variables; $F(U) = [\rho u, \rho u^2 + p, \rho uv, u(E + p)]^T$ and $G(U) = [\rho v, \rho uv, \rho v^2 + p, v(E + p)]^T$ denote the inviscid fluxes; ρ is the fluid density; u and v are the velocity components in the x and y directions, respectively; E is the total energy per unit volume; and p is the pressure satisfying $p = (\gamma - 1)(E - \frac{\rho(u^2+v^2)}{2})$, with the specific heat ratio $\gamma = 1.4$. Due to the potential occurrence of shocks and contact discontinuities in solutions of the Euler equations, both exact solutions and numerical simulations present significant challenges.

Among high-order accurate schemes, the weighted essentially non-oscillatory (WENO) scheme [1] has become an ideal choice for solving Euler equations because it maintains essentially non-oscillatory properties near discontinuities while achieving high-order accuracy in smooth regions. Compared to the essentially non-oscillatory (ENO) scheme [2] that reconstructs numerical fluxes using optimal stencil information, the WENO scheme introduces nonlinear weighting technology that utilizes information from all candidate stencils, yielding higher accuracy in smooth regions and better stability near discontinuities. Jiang and Shu [3] constructed sub-stencil smoothness indicators and proposed the fifth-order WENO-JS scheme. To address the accuracy degradation issue of WENO-JS near extrema, numerous improvements have been proposed in the literature [4-12]. For instance, Henrick et al. [4] introduced a mapped weighting function to modify nonlinear weights, resulting in the WENO-M scheme that achieves optimal accuracy near extrema but significantly increases computational cost due to the mapping function. Borges et al. [5] designed a new Z-type weighting factor by defining a global smoothness indicator, leading to the WENO-Z scheme that maintains optimal accuracy near extrema with computational efficiency comparable to WENO-JS. Xu et al. [6] developed a conservative hybrid central-WENO scheme using weighted averaging of third-order WENO and second-order central schemes. Luo and Wu [7] further improved scheme resolution by adjusting weights on under-smooth substencils. Hu et al. [8] proposed the adaptive central-upwind WENO-CU6 scheme based on a strategy of adaptively selecting central or upwind stencils, which employs central stencils in smooth regions for low-dissipation characteristics and upwind stencils near discontinuities for numerical stability. Huang et al. [9] improved the WENO-CU6 scheme by using one six-point stencil and three three-point stencils for reconstruction, with flexible linear weights (any positive numbers summing to one), and introduced a new smoothness indicator. Zhu et al. [10-11] constructed the WENO-ZQ scheme using one five-point stencil and two two-point stencils, and the multi-resolution WENO-ZS scheme with nested stencils. Balsara et al. [12] designed the WENO-AO scheme based on the interpolation concept of WENO-ZQ, where smoothness indicators take the form of complete squares.

The weighted compact nonlinear scheme (WCNS) represents another high-order, high-resolution method for solving Euler equations [13-29]. Deng and Zhang [13-15] introduced the nonlinear WENO interpolation concept into compact nonlinear schemes, proposing the WCNS scheme characterized by high resolution and strong discontinuity-capturing capability. Zhang et al. [16] and Nonomura et al. [17-18] extended the WCNS scheme to higher orders and demonstrated its excellent performance through numerical experiments. Nonomura et al. [17-18] confirmed that WCNS not only inherits the advantages of WENO schemes but also offers three additional benefits: higher resolution, compatibility with various flux splitting formulations, and outstanding free-stream and vortex-preserving properties on curvilinear grids. Deng et al. [19] constructed a hybrid cell-edge and cell-node WCNS scheme, verifying that it uses a more compact stencil than classical WCNS schemes of the same order and provides higher

resolution near discontinuities. Tu et al. [20] confirmed through approximate dispersion relation analysis that WCNS schemes exhibit better spectral characteristics than WENO schemes. Wong et al. [21] proposed the locally dissipative weighted compact scheme (WCNS-LD). Kamiya et al. [22-23] constructed the WCNS-CU6-Z and EWCNS-CU4 schemes with adaptive central-upwind characteristics based on the adaptive upwind concept from WENO-CU schemes. Yan et al. [24] proposed Y-type nonlinear weights for WCNS schemes to improve shock-capturing capability. Subramaniam et al. [25] improved WCNS schemes by designing low-dispersion high-order formulations. Hiejima [26] developed the WCNS-T scheme inspired by TENO ideas, which effectively captures both high-frequency waves and strong shocks. Fan et al. [27] designed WCNS schemes for solving shallow water equations with source terms. Jiang et al. [28] proposed high-order semi-implicit WCNS schemes to avoid the strict CFL stability limitations of explicit WCNS schemes and improve computational efficiency.

This study draws inspiration from the WENO-AO interpolation concept in [12] to construct the WCNS-AO scheme that blends low-order interpolations on three-point substencils with high-order interpolation on a global five-point stencil for solving Euler equations. The WCNS-AO spatial discretization combines a hybrid cell-edge and cell-node sixth-order central differencing scheme for flux derivative calculation with an adaptive-order nonlinear weighted interpolation method based on characteristic projection. To verify the performance of the WCNS-AO scheme, it is combined with high-order TVD Runge-Kutta time discretization [3] and applied to one- and two-dimensional test cases, with comparisons made against the classical fifth-order WCNS-Z and fifth-order WENO-AO schemes.

---

1 Numerical Methods

This section presents the derivation of the fifth-order WCNS-AO scheme using the one-dimensional Euler equations as an example. The multidimensional case can be derived similarly through a dimension-by-dimension approach. The one-dimensional Euler equations are given by

$$\frac{\partial U}{\partial t} + \frac{\partial F(U)}{\partial x} = 0$$

where U_i and F_i' represent approximations of the unknown variables U and flux derivatives $\partial F/\partial x$ at node x_i, respectively.

1.1 Sixth-Order Central Differencing Scheme

Based on the classical fifth-order WCNS scheme, the flux derivative F' is computed using a hybrid cell-edge and cell-node central differencing scheme [20]. The general form is

$$\alpha F'_{i-1}+F'_i+\alpha F'_{i+1}=\frac{a}{h}(F_{i+1/2}-F_{i-1/2})+\frac{b}{h}(F_{i+3/2}-F_{i-3/2})+\frac{c}{h}(F_{i+5/2}-F_{i-5/2})$$

where the scheme is termed implicit when parameter $\alpha \neq 0$ and explicit otherwise. Taylor series expansion of Eq. (4) yields relationships between the scheme's order of accuracy and the four coefficients α, a, b, c. Generally, implicit and explicit schemes do not produce significantly different numerical results [17]. Clearly, explicit schemes offer higher computational efficiency as they avoid solving tridiagonal linear systems for flux derivative approximation. Therefore, this study employs the following sixth-order explicit scheme for flux derivative calculation:

$$F'_i=\frac{9}{8h}(F_{i+1/2}-F_{i-1/2})-\frac{1}{24h}(F_{i+3/2}-F_{i-3/2})$$

Here, $F_{i\pm1/2}$ represents numerical approximations of fluxes at half-nodes $x_{i\pm1/2}$, obtained through characteristic projection-based nonlinear weighted interpolation.

1.2 Characteristic Projection Method

The Jacobian matrix of flux F is defined as

$$A=\frac{\partial F}{\partial U}=\begin{pmatrix} 0 & 1 & 0 & 0 \\ \frac{\gamma-3}{2}u^2 & (3-\gamma)u & \gamma-1 & 0 \\ -uv & v & u & 0 \\ \frac{\gamma-1}{2}u^3-uH & H-(\gamma-1)u^2 & (\gamma-1)u & u \end{pmatrix}$$

where $c=\sqrt{\gamma p/\rho}$ denotes the speed of sound. The Jacobian matrix A is decomposed as $A=R\Lambda L$, where $\Lambda=\mathrm{diag}[u-c,u,u+c]$ is the eigenvalue matrix, and L and R are the left and right eigenvector matrices, respectively:

$$L=\begin{pmatrix} \frac{\gamma-1}{2}\frac{u^2}{c^2}-\frac{u}{c} & -\frac{\gamma-1}{c^2}u+\frac{1}{c} & \frac{\gamma-1}{c^2} & -\frac{\gamma-1}{c^2} \\ 1-\frac{\gamma-1}{2}\frac{u^2}{c^2} & \frac{\gamma-1}{c^2}u & -\frac{\gamma-1}{c^2} & \frac{\gamma-1}{c^2} \\ \frac{\gamma-1}{2}\frac{u^2}{c^2}+\frac{u}{c} & -\frac{\gamma-1}{c^2}u-\frac{1}{c} & \frac{\gamma-1}{c^2} & -\frac{\gamma-1}{c^2} \end{pmatrix}$$

$$R=\begin{pmatrix} 1 & 1 & 1 \\ u-c & u & u+c \\ H-uc & \frac{u^2}{2} & H+uc \end{pmatrix}$$

where $\lambda=\max\{|u+c|,|u-c|\}$ represents the maximum characteristic speed.

To enhance scheme stability, the Lax-Friedrichs flux splitting technique is employed to decompose the flux F_i at each node into positive and negative components: $F_i^+ = (F_i + \lambda U_i)/2$ and $F_i^- = (F_i - \lambda U_i)/2$, where λ is the maximum eigenvalue of the Jacobian matrix A. The calculation process for $F_{i+1/2}^+$ is presented below, while $F_{i+1/2}^-$ follows a symmetric procedure about half-node $x_{i+1/2}$ and is omitted for brevity. For derivation simplicity, the superscript "+" is also omitted. The numerical flux at half-node $x_{i+1/2}$ is computed as $F_{i+1/2}$.

To effectively eliminate non-physical oscillations near discontinuities, this study employs characteristic projection-based nonlinear weighted interpolation. First, the flux F_i at each node is projected into characteristic space to obtain characteristic fluxes $W_i = L_{i+1/2}F_i$. The numerical characteristic flux $W_{i+1/2}$ is then solved using nonlinear weighted interpolation in characteristic space and projected back to physical space to obtain $F_{i+1/2}$. The left and right eigenvector matrices $L_{i+1/2}$ and $R_{i+1/2}$ at half-node $x_{i+1/2}$ are obtained through arithmetic averaging of adjacent node values.

1.3 WCNS-AO Scheme

To achieve fifth-order accuracy in the WCNS-AO scheme, a five-point stencil $S = [x_{i-2}, x_{i-1}, x_i, x_{i+1}, x_{i+2}]$ is used to compute the numerical characteristic flux $w_{i+1/2}$ at half-node $x_{i+1/2}$. Taking one component w of W as an example, the nonlinear weighted interpolation process for $w_{i+1/2}$ is presented; other components follow analogously.

A fourth-degree Lagrange interpolation polynomial $p(x)$ is constructed based on stencil S to obtain the fifth-order numerical flux:

$$w_{i+1/2} = \frac{1}{128}(-3w_{i-2} + 20w_{i-1} + 90w_i + 60w_{i+1} - 5w_{i+2})$$

This expression can also be obtained through linear weighting of third-order numerical fluxes on three substencils of S. The substencils are defined as $S_k = [x_{i+k-2}, x_{i+k-1}, x_{i+k}]$ for $k = 0, 1, 2$. Quadratic Lagrange interpolation polynomials $p_k(x)$ are constructed on each S_k to yield third-order numerical fluxes:

$$w_{i+1/2,0} = \frac{1}{8}(3w_{i-2} + 10w_{i-1} + 15w_i)$$

$$w_{i+1/2,1} = \frac{1}{8}(-w_{i-1} + 6w_i + 3w_{i+1})$$

$$w_{i+1/2,2} = \frac{1}{8}(3w_i + 6w_{i+1} - w_{i+2})$$

The high-order numerical flux $w_{i+1/2}$ can be expressed as a linear combination of these low-order fluxes:

$$w_{i+1/2} = d_0 w_{i+1/2,0} + d_1 w_{i+1/2,1} + d_2 w_{i+1/2,2}$$

where the linear weights are $d_0 = 1/16$, $d_1 = 10/16$, and $d_2 = 5/16$.

To improve the resolution and shock-capturing performance of the original fifth-order WCNS-Z scheme, this study adopts the WENO-AO nonlinear interpolation concept [12], employing a nonlinear weighted interpolation technique that blends low-order interpolations on substencils with high-order interpolation on the global stencil to compute $w_{i+1/2}$. The numerical flux calculation in Eq. (9) is reformulated as:

$$w_{i+1/2} = d_3 w^{(4)}_{i+1/2} + \sum_{k=0}^{2} d_k w_{i+1/2,k}$$

where d_k are arbitrary positive numbers satisfying $\sum_{k=0}^{3} d_k = 1$. In this study, the values are chosen as $d_0 = d_2 = (1-\alpha)(1-d_3)/2$, $d_1 = \alpha(1-d_3)$, with $\alpha = 0.95$ and $d_3 = 0.95$.

While linear weights yield high-order schemes, they produce numerical oscillations near discontinuities. To address this, the WENO nonlinear interpolation concept is introduced, where nonlinear weights replace linear weights to achieve high-order accuracy in smooth regions while avoiding interpolation across discontinuities. Various definitions of nonlinear weights have been proposed in [4-7], among which Z-type weights (from WENO-Z [5]) are particularly popular. To obtain the nonlinear weighted form of Eq. (12), smoothness indicators for each stencil are first defined. For WCNS schemes using interpolation-type numerical fluxes, smoothness indicators on each stencil can be defined as complete square sums of interpolation polynomial derivatives [14]. The smoothness indicator β_k for substencil S_k is defined as $\beta_k = (hp'_k)^2 + (h^2 p''_k)^2$ for $k = 0, 1, 2$, while the smoothness indicator β_3 for global stencil S is defined as $\beta_3 = (hp')^2 + (h^2 p'')^2 + (h^3 p^{(3)})^2 + (h^4 p^{(4)})^2$. The explicit expressions are:

$$\beta_0 = \frac{1}{4}(w_{i-2} - 4w_{i-1} + 3w_i)^2 + (w_{i-2} - 2w_{i-1} + w_i)^2$$

$$\beta_1 = \frac{1}{4}(w_{i-1} - w_{i+1})^2 + (w_{i-1} - 2w_i + w_{i+1})^2$$

$$\beta_2 = \frac{1}{4}(3w_i - 4w_{i+1} + w_{i+2})^2 + (w_i - 2w_{i+1} + w_{i+2})^2$$

$$\beta_3 = \frac{1}{144}(w_{i-2}-8w_{i-1}+8w_{i+1}-w_{i+2})^2+\frac{1}{144}(-w_{i-2}+16w_{i-1}-20w_i+16w_{i+1}-w_{i+2})^2+\frac{1}{4}(-w_{i-2}+2w_{i-1}-2w_{i+1}+$$

The global smoothness indicator τ is defined as:

$$\tau = \left(|\beta_3 - \beta_0| + |\beta_3 - \beta_1| + |\beta_3 - \beta_2|\right)^3$$

The Z-type weights from [5] are adopted to compute nonlinear weights ω_k:

$$\alpha_k = d_k \left(1 + \frac{\tau}{\beta_k + \epsilon}\right)^2, \quad \omega_k = \frac{\alpha_k}{\sum_{j=0}^{3} \alpha_j}$$

Replacing linear weights d_k in Eq. (12) with nonlinear weights ω_k yields the WCNS-AO scheme, where the nonlinear interpolation formula for numerical flux $w_{i+1/2}$ becomes:

$$w_{i+1/2} = \omega_3 w^{(4)}_{i+1/2} + \sum_{k=0}^{2} \omega_k w_{i+1/2,k}$$

Taylor expansions of the smoothness indicators at point x_i give:

$$\beta_k = h^2 (w_i')^2 \left[1 + O(h^2)\right], \quad \tau = O(h^4) \quad \text{when } w_i' \neq 0$$

$$\beta_k = h^4 (w_i'')^2 \left[1 + O(h^2)\right], \quad \tau = O(h^4) \quad \text{when } w_i' = 0$$

Substituting these into Eq. (15) yields $\omega_k = d_k + O(h^4)$. The nonlinear interpolation formula can be rewritten as:

$$w_{i+1/2} = \omega_3 w^{(4)}_{i+1/2} + \sum_{k=0}^{2} \omega_k w_{i+1/2,k} = w_{i+1/2} + A(h^5) + O(h^6) + (\omega_3 - d_3)[A(h^5) + O(h^6)] - (\omega_3 - d_3) \sum_{k=0}^{2} [B_k(h^3) + O(h$$

where A and B_k are constants. Combining these results proves that the nonlinear interpolation formulation achieves fifth-order accuracy.

1.4 Time Discretization

After spatial discretization of the Euler equations using the WCNS-AO scheme, a system of ordinary differential equations in time is obtained:

$$\frac{dU}{dt} = L(U)$$

where L represents the spatial discretization operator. The third-order explicit TVD Runge-Kutta method is employed to solve Eq. (22):

$$U^{(1)} = U^n + \Delta t L(U^n)$$

$$U^{(2)} = \frac{3}{4}U^n + \frac{1}{4}U^{(1)} + \frac{1}{4}\Delta t L(U^{(1)})$$

$$U^{n+1} = \frac{1}{3}U^n + \frac{2}{3}U^{(2)} + \frac{2}{3}\Delta t L(U^{(2)})$$

where Δt is the time step size.

---

2 Numerical Experiments

This section validates the performance of the fifth-order WCNS-AO scheme through several numerical experiments and compares it with the fifth-order WCNS scheme [28] and fifth-order WENO-AO scheme [12].

2.1 Accuracy Test Case

Consider the one-dimensional Euler equations with initial conditions $\rho(x, 0) = 2 + \sin[x - \sin(x)]$, $u = 1$, and $p = 1$. The exact solution is $\rho(x, t) = 2 + \sin[(x - t) - \sin(x - t)]$. The computational domain is $[0, 2\pi]$ with periodic boundary conditions, and the final simulation time is $t = 2.0$ s. To eliminate the influence of time discretization on spatial accuracy, the time step is set as $\Delta t = (\Delta x)^{5/3}$. presents the L_1 and L_∞ numerical errors, convergence rates, and CPU time T_{CPU} for both WCNS-AO and WENO-AO schemes. The results show that WCNS-AO exhibits better convergence than WENO-AO for this case and achieves fifth-order accuracy in smooth regions.

For the two-dimensional Euler equations, initial conditions are set as $\rho(x, y, 0) = 1 + 0.2\sin(x + y)$, $u = v = 1$, and $p = 1$. The exact solution is $\rho(x, y, t) = 1 + 0.2\sin(x + y - 2t)$. The computational domain is $[0, 2\pi]^2$ with periodic boundaries, and the final time is $t = 2.0$ s. provides the L_1 and L_∞ errors, convergence rates, and CPU time for both schemes. Both achieve fifth-order

accuracy in smooth regions, with WCNS-AO producing smaller numerical errors than WENO-AO. [FIGURE:1] shows the relationship between L_1 errors and CPU time for both schemes. The results indicate comparable computational efficiency for the one-dimensional case, while WCNS-AO is slightly more efficient than WENO-AO for the two-dimensional problem.

2.2 Lax Problem

This classical one-dimensional Riemann problem, featuring rarefaction waves and shocks, is commonly used to test shock-capturing capability. The initial conditions are

$$(\rho, u, p) = \begin{cases} (0.445, 0.698, 3.528), & -0.5 < x \leq 0 \\ (0.5, 0.0, 0.571), & 0 < x < 0.5 \end{cases}$$

The computational domain is $[-0.5, 0.5]$ with compact boundary conditions, using $N = 201$ grid points and final time $t = 0.13$ s.

compares numerical results from the fifth-order WCNS, WENO-AO, and WCNS-AO schemes against a reference solution obtained with a fine grid ($N = 5000$) using WENO. Both WCNS and WENO-AO produce noticeable numerical oscillations near the shock, while WCNS-AO performs best by effectively suppressing oscillations and demonstrating stronger shock-capturing capability.

2.3 Sod Problem

This classical one-dimensional Riemann problem is commonly used to test scheme stability. The initial conditions are

$$(\rho, u, p) = \begin{cases} (1.0, 0.0, 1.0), & -0.5 < x \leq 0 \\ (0.125, 0.0, 0.1), & 0 < x < 0.5 \end{cases}$$

The computational domain is $[-0.5, 0.5]$ with compact boundary conditions, using $N = 201$ grid points and final time $t = 0.13$ s.

compares numerical results from the three schemes against a reference solution. All three schemes demonstrate good stability, with WCNS-AO showing optimal shock-capturing performance and better stability.

2.4 Osher-Shu Problem

This problem exhibits high-frequency oscillatory characteristics and is often used to test scheme accuracy and dissipative errors. The initial conditions are

$$(\rho, u, p) = \begin{cases} (3.857143, 2.699369, 10.33333), & -5 < x \leq -4 \\ (1 + 0.2\sin(5x), 0.0, 1.0), & -4 < x < 5 \end{cases}$$

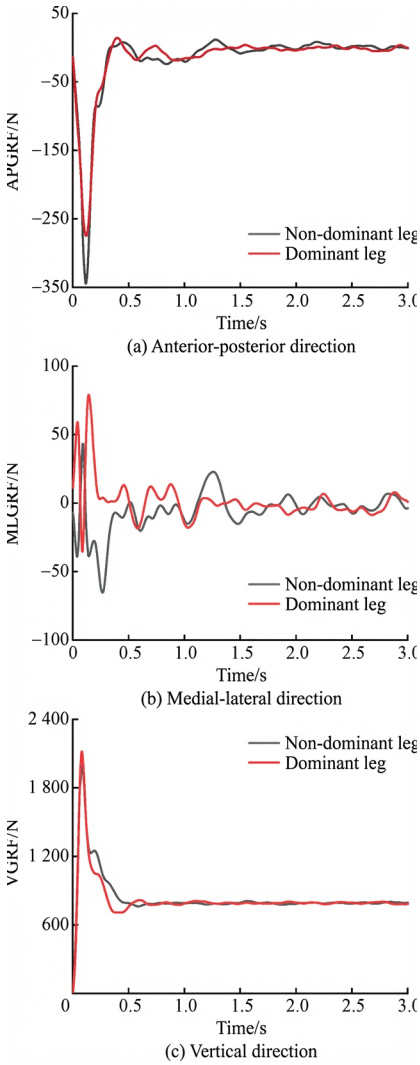

Figure 1: Figure 2

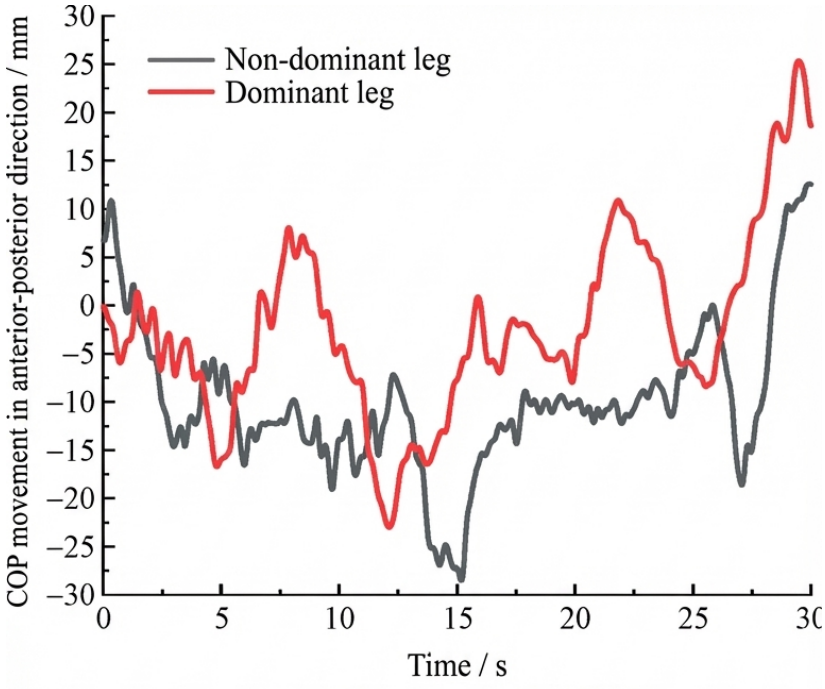

(a) Anterior-posterior direction

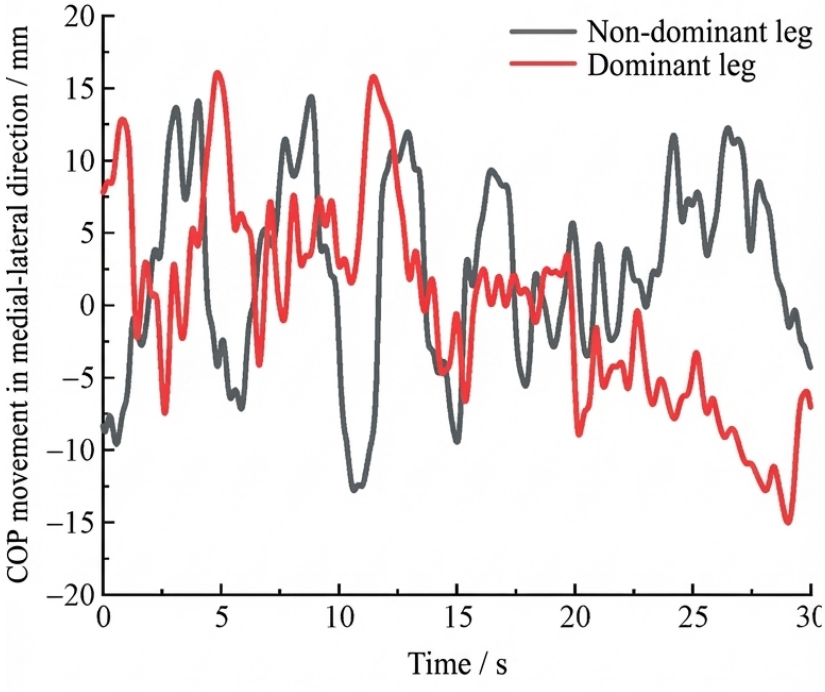

(b) Medial-lateral direction

Figure 2: Figure 3

The computational domain is $[-0.5, 0.5]$ with compact boundary conditions, using 201×201 grid points and final time $t = 1.8$ s. [FIGURE:4] presents numerical results from the three schemes compared with a reference solution. The results show that WCNS-AO performs better than WCNS and WENO-AO at acoustic-entropy wave interfaces, demonstrating stronger high-frequency wave-capturing capability and higher resolution.

2.5 Two-Dimensional Riemann Problem

This problem contains numerous flow structures and serves as a comprehensive test for stability, dissipation, resolution, and shock-capturing capability. The initial conditions in domain $[0, 1]^2$ are [7]:

$$(\rho, u, v, p) = \begin{cases} (1.5, 0.0, 0.0, 1.5), & x \geq 0.8, y \geq 0.8 \\ (0.5323, 1.203, 0.0, 0.3), & x < 0.8, y \geq 0.8 \\ (0.138, 1.206, 1.206, 0.029), & x < 0.8, y < 0.8 \\ (0.5323, 0.0, 1.206, 0.3), & x \geq 0.8, y < 0.8 \end{cases}$$

Dirichlet boundary conditions are applied on a 401×401 grid with final time $t = 0.8$ s. [FIGURE:5] shows density distributions from the three schemes with 30 contour lines ranging from 0.1 to 1.8. All schemes capture most vortex structures, but WCNS-AO performs better by resolving finer vortical structures with reduced dissipation and improved resolution compared to WCNS and WENO-AO.

2.6 Double Mach Reflection Problem

This problem describes a Mach 10 oblique shock impinging on an inviscid wall at a 60° angle, creating complex flow phenomena involving shock reflection and vortical structures. It is commonly used to test shock and small-scale structure capturing capabilities. The computational domain is $[0, 3] \times [0, 1]$ with initial conditions [30]:

$$(\rho, u, v, p) = \begin{cases} (8.0, 8.25\cos(\pi/6), -8.25\sin(\pi/6), 116.5), & x < 1/6 + y/\sqrt{3} \\ (1.4, 0.0, 0.0, 1.0), & x \geq 1/6 + y/\sqrt{3} \end{cases}$$

Inflow boundary conditions are applied on the left and bottom ($0 < x \leq 1/6$) boundaries; reflection conditions on the bottom ($x > 1/6$); outflow conditions on the right; and exact solution on the top boundary. The grid size is 961×241 with final time $t = 0.2$ s. [FIGURE:6] presents density distributions with 30 contour lines from 1.4 to 21.6711. All three schemes capture shock information in the flow field, but WCNS-AO resolves finer vortical structures in the roll-up region with smaller numerical dissipation and better resolution compared to WCNS and WENO-AO.

2.7 Rayleigh-Taylor Instability Problem

This problem involves instability at the interface between two fluids of different densities. The computational domain is $[0, 0.25] \times [0, 1]$ with initial conditions [31]:

$$(\rho, u, v, p) = \begin{cases} (2.0, 0.0, -0.025a\cos(8\pi x), 2y + 1), & 0 \le y < 0.5 \\ (1.0, 0.0, -0.025a\cos(8\pi x), y + 1.5), & 0.5 < y \le 1 \end{cases}$$

where $a = 0.5$. The specific heat ratio is $\gamma = 5/3$. Reflective boundary conditions are applied on left and right boundaries, with top conditions $(\rho, u, v, p) = (1.0, 0.0, 0.0, 2.5)$ and bottom conditions $(\rho, u, v, p) = (2.0, 0.0, 0.0, 1.0)$. The grid size is 241×961 with final time $t = 1.95$ s. [FIGURE:7] shows density distributions from the three schemes. WCNS-AO outperforms WCNS by capturing small vortices induced by RT instability at the density interface. In this case, WENO-AO produces slightly better results than WCNS-AO with minimal numerical dissipation, but WCNS-AO still shows improved performance over WCNS.

Conclusion

This study constructs a WCNS-AO scheme based on adaptive-order interpolation for solving Euler equations. The scheme combines a hybrid cell-edge and cell-node sixth-order central differencing scheme for computing spatial derivatives of fluxes at cell nodes with an adaptive-order nonlinear interpolation method for numerical fluxes at half-nodes. Flux splitting techniques and characteristic projection are employed to enhance scheme stability and effectively eliminate non-physical oscillations near discontinuities. Combined with third-order TVD Runge-Kutta time discretization, the newly designed fifth-order WCNS-AO scheme is applied to one- and two-dimensional Euler equations and compared with classical fifth-order WCNS and fifth-order WENO-AO schemes.

Numerical results demonstrate that WCNS-AO achieves the designed fifth-order accuracy in smooth regions with computational efficiency slightly higher than WENO-AO. One-dimensional test cases (Lax and Sod problems) verify that WCNS-AO exhibits optimal shock-capturing capability and better stability compared to WCNS and WENO-AO schemes of the same order. Two-dimensional Riemann and double Mach reflection problems confirm that WCNS-AO outperforms WCNS and WENO-AO by capturing finer flow structures with reduced numerical dissipation and improved resolution. For the Rayleigh-Taylor instability problem, while WENO-AO performs slightly better than WCNS-AO, WCNS-AO still shows superior performance compared to WCNS, thereby improving the dissipative characteristics of the original scheme.

References

[1] Liu X D, Osher S, Chan T. Weighted essentially non-oscillatory schemes[J]. Journal of computational physics, 1994, 115(1): 200-212.
[2] Shu C W, Osher S. Efficient implementation of essentially non-oscillatory shock-capturing schemes[J]. Journal of computational physics, 1988, 77(2): 439-471.
[3] Jiang G S, Shu C W. Efficient implementation of weighted ENO schemes[J]. Journal of computational physics, 1996, 126(1): 202-228.
[4] Henrick A K, Aslam T D, Powers J M. Mapped weighted essentially non-oscillatory schemes: achieving optimal order near critical points[J]. Journal of computational physics, 2005, 207(2): 542-567.
[5] Borges R, Carmona M, Costa B, et al. An improved weighted essentially non-oscillatory scheme for hyperbolic conservation laws[J]. Journal of computational physics, 2008, 227(6): 3191-3211.
[6] Xu W Z, Kong X S, Zheng C, et al. An improved hybrid central-WENO scheme[J]. Chinese journal of applied mechanics, 2017, 34(6): 1115-1119 (in Chinese).
[7] Luo X, Wu S P. An improved fifth-order WENO-Z+ scheme[J]. Chinese journal of theoretical and applied mechanics, 2019, 51(6): 1927-1939 (in Chinese).
[8] Hu X Y, Wang Q, Adams N A. An adaptive central-upwind weighted essentially non-oscillatory scheme[J]. Journal of computational physics, 2010, 229(23): 8952-8965.
[9] Huang C, Chen L L. A new adaptively central-upwind sixth-order WENO scheme[J]. Journal of computational physics, 2018, 357: 1-15.
[10] Zhu J, Qiu J X. A new fifth order finite difference WENO scheme for solving hyperbolic conservation laws[J]. Journal of computational physics, 2016, 318: 110-121.
[11] Zhu J, Shu C W. A new type of multi-resolution WENO schemes with increasingly higher order of accuracy[J]. Journal of computational physics, 2018, 375: 659-683.
[12] Balsara D S, Garain S, Shu C W. An efficient class of WENO schemes with adaptive order[J]. Journal of computational physics, 2016, 326: 780-804.
[13] Deng X G, Zhang H X. Developing high-order weighted compact nonlinear schemes[J]. Journal of computational physics, 2000, 165(1): 22-44.
[14] Deng X G. High-order dissipative weighted compact nonlinear scheme[J]. Science in China (series A), 2001, 31(12): 1104-1117 (in Chinese).
[15] Deng X G, Maekawa H. Compact high-order accurate nonlinear schemes[J]. Journal of computational physics, 1997, 130(1): 77-91.
[16] Zhang S H, Jiang S F, Shu C W. Development of nonlinear weighted compact schemes with increasingly higher order accuracy[J]. Journal of computational physics, 2008, 227(15): 7294-7321.
[17] Nonomura T, Fujii K. Effects of difference scheme type in high-order weighted compact nonlinear schemes[J]. Journal of computational physics, 2009, 228(10): 3533-3539.

[18] Nonomura T, Fujii K. Robust explicit formulation of weighted compact nonlinear scheme[J]. Computers & fluids, 2013, 85: 8-15.
[19] Deng X G, Jiang Y, Mao M L, et al. A family of hybrid cell-edge and cell-node dissipative compact schemes satisfying geometric conservation law[J]. Computers & fluids, 2015, 116: 29-45.
[20] Tu G H, Deng X G, Mao M L. Spectral property comparison of fifth-order nonlinear WCNS and WENO difference schemes[J]. Acta aerodynamica Sinica, 2012, 30(6): 709-712 (in Chinese).
[21] Wong M L, Lele S K. High-order localized dissipation weighted compact nonlinear scheme for shock- and interface-capturing in compressible flows[J]. Journal of computational physics, 2017, 339: 179-209.
[22] Kamiya T, Asahara M, Nonomura T. Application of central differencing and low-dissipation weights in a weighted compact nonlinear scheme[J]. International journal for numerical methods in fluids, 2017, 84(3): 152-180.
[23] Zhao G Y, Sun M B, Xie S B, et al. Numerical dissipation control in an adaptive WCNS with a new smoothness indicator[J]. Applied mathematics and computation, 2018, 330: 239-253.
[24] Yan Z G, Liu H Y, Ma Y K, et al. Further improvement of weighted compact nonlinear scheme using compact nonlinear interpolation[J]. Computers & fluids, 2017, 156: 135-145.
[25] Subramaniam A, Wong M L, Lele S K. A high-order weighted compact high resolution scheme with boundary closures for compressible turbulent flows with shocks[J]. Journal of computational physics, 2019, 397: 108822.
[26] Hiejima T. A high-order weighted compact nonlinear scheme for compressible flows[J]. Computers & fluids, 2022, 232: 105199.
[27] Fan R, Chen X, Zheng K L, et al. High order implicit WCNS scheme for the shallow water equations[J]. Chinese journal of applied mechanics, 2021, 38(4): 1477-1484 (in Chinese).
[28] Jiang Y Q, Zhou S G, Zhang X, et al. High order all-speed semi-implicit weighted compact nonlinear scheme for the isentropic Navier-Stokes equations[J]. Journal of computational and applied mathematics, 2022, 411: 114272.
[29] Hu Y G, Jiang Y Q, Huang X Q. High order weight compact nonlinear scheme for time-dependent Hamilton-Jacobi equations[J]. Chinese journal of theoretical and applied mechanics, 2022, 54(11): 3203-3214 (in Chinese).
[30] Woodward P, Colella P. The numerical simulation of two-dimensional fluid flow with strong shocks[J]. Journal of computational physics, 1984, 54(1): 115-173.
[31] Shi J, Zhang Y T, Shu C W. Resolution of high order WENO schemes for complicated flow structures[J]. Journal of computational physics, 2003, 186(2): 690-696.